Frequency-modulated light scattering interferometry employed for optical properties and dynamics studies of turbid media.

Mei, Liang; Somesfalean, Gabriel; Svanberg, Sune

Published in:
Biomedical Optics Express

DOI:
10.1364/BOE.5.002810

2014

Biomedical Optics EXPRESS

Frequency-modulated light scattering interferometry employed for optical properties and dynamics studies of turbid media

Liang Mei,[1] Gabriel Somesfalean,[1] and Sune Svanberg[1,2]

[1]*Atomic Physics Division, Department of Physics, Lund University, P.O. Box 118, SE-221 00 Lund, Sweden*
[2]*Centre for Optical and Electromagnetic Research, South China Normal University, 510006 Guangzhou, China*
**liang.mei@fysik.lth.se*

Abstract: In the present work, fiber-based frequency-modulated light scattering interferometry (FMLSI) is developed and employed for studies of optical properties and dynamics in liquid phantoms made from Intralipid®. The fiber-based FMLSI system retrieves the optical properties by examining the intensity fluctuations through the turbid medium in a heterodyne detection scheme using a continuous-wave frequency-modulated coherent light source. A time resolution of 21 ps is obtained, and the experimental results for the diluted Intralipid phantoms show good agreement with the predicted results based on published data. The present system shows great potential for assessment of optical properties as well as dynamic studies in liquid phantoms, dairy products, and human tissues.

OCIS codes: (290.7050) Turbid media; (120.5820) Scattering measurements; (120.6160) Speckle interferometry.

References and links

1. Z. Q. Shi and C. A. Anderson, "Pharmaceutical applications of separation of absorption and scattering in near-infrared spectroscopy (NIRS)," J. Pharm. Sci. **99**(12), 4766–4783 (2010).
2. D. Khoptyar, A. A. Subash, S. Johansson, M. Saleem, A. Sparén, J. Johansson, and S. Andersson-Engels, "Broadband photon time-of-flight spectroscopy of pharmaceuticals and highly scattering plastics in the VIS and close NIR spectral ranges," Opt. Express **21**(18), 20941–20953 (2013).
3. I. Bargigia, A. Nevin, A. Farina, A. Pifferi, C. D'Andrea, M. Karlsson, P. Lundin, G. Somesfalean, and S. Svanberg, "Diffuse optical techniques applied to wood characterisation," J. Near Infrared Spectrosc. **21**(4), 259–268 (2013).
4. T. L. Troy and S. N. Thennadil, "Optical properties of human skin in the near infrared wavelength range of 1000 to 2200 nm," J. Biomed. Opt. **6**(2), 167–176 (2001).
5. E. Salomatina, B. Jiang, J. Novak, and A. N. Yaroslavsky, "Optical properties of normal and cancerous human skin in the visible and near-infrared spectral range," J. Biomed. Opt. **11**(6), 064026 (2006).
6. T. Lister, P. A. Wright, and P. H. Chappell, "Optical properties of human skin," J. Biomed. Opt. **17**(9), 090901 (2012).
7. S. H. Chung, A. E. Cerussi, C. Klifa, H. M. Baek, O. Birgul, G. Gulsen, S. I. Merritt, D. Hsiang, and B. J. Tromberg, "In vivo water state measurements in breast cancer using broadband diffuse optical spectroscopy," Phys. Med. Biol. **53**(23), 6713–6727 (2008).
8. A. J. Lin, M. A. Koike, K. N. Green, J. G. Kim, A. Mazhar, T. B. Rice, F. M. LaFerla, and B. J. Tromberg, "Spatial frequency domain imaging of intrinsic optical property contrast in a mouse model of Alzheimer's disease," Ann. Biomed. Eng. **39**(4), 1349–1357 (2011).
9. S. Fantini and A. Sassaroli, "Near-infrared optical mammography for breast cancer detection with intrinsic contrast," Ann. Biomed. Eng. **40**(2), 398–407 (2012).
10. J. L. Sandell and T. C. Zhu, "A review of in-vivo optical properties of human tissues and its impact on PDT," J. Biophotonics **4**(11-12), 773–787 (2011).
11. S. L. Jacques, "Optical properties of biological tissues: a review," Phys. Med. Biol. **58**(11), R37–R61 (2013).
12. B. C. Wilson, E. M. Sevick, M. S. Patterson, and B. Chance, "Time-dependent optical spectroscopy and imaging for biomedical applications," Proceedings of the IEEE (1992).
13. B. J. Tromberg, O. Coquoz, J. B. Fishkin, T. Pham, E. R. Anderson, J. Butler, M. Cahn, J. D. Gross, V. Venugopalan, and D. Pham, "Non-invasive measurements of breast tissue optical properties using frequency-domain photon migration," Philos. Trans. R. Soc. Lond. B Biol. Sci. **352**(1354), 661–668 (1997).

#211079 - $15.00 USD Received 29 Apr 2014; revised 29 Jun 2014; accepted 30 Jun 2014; published 28 Jul 2014

14. R. M. P. Doornbos, R. Lang, M. C. Aalders, F. W. Cross, and H. J. C. M. Sterenborg, "The determination of in vivo human tissue optical properties and absolute chromophore concentrations using spatially resolved steady-state diffuse reflectance spectroscopy," Phys. Med. Biol. **44**(4), 967–981 (1999).
15. L. Mei, S. Svanberg, and G. Somesfalean, "Combined optical porosimetry and gas absorption spectroscopy in gas-filled porous media using diode-laser-based frequency domain photon migration," Opt. Express **20**(15), 16942–16954 (2012).
16. J. M. Schmitt, A. Knüttel, and R. F. Bonner, "Measurement of optical properties of biological tissues by low-coherence reflectometry," Appl. Opt. **32**(30), 6032–6042 (1993).
17. A. I. Kholodnykh, I. Y. Petrova, K. V. Larin, M. Motamedi, and R. O. Esenaliev, Optimization of low coherence interferometry for quantitative analysis of tissue optical properties, Optical Diagnostics and Sensing of Biological Fluids and Glucose and Cholesterol Monitoring II (2002).
18. A. I. Kholodnykh, I. Y. Petrova, K. V. Larin, M. Motamedi, and R. O. Esenaliev, "Precision of measurement of tissue optical properties with optical coherence tomography," Appl. Opt. **42**(16), 3027–3037 (2003).
19. T. Gambichler, G. Moussa, M. Sand, D. Sand, P. Altmeyer, and K. Hoffmann, "Applications of optical coherence tomography in dermatology," J. Dermatol. Sci. **40**(2), 85–94 (2005).
20. V. Turzhitsky, A. J. Radosevich, J. D. Rogers, N. N. Mutyal, and V. Backman, "Measurement of optical scattering properties with low-coherence enhanced backscattering spectroscopy," J. Biomed. Opt. **16**(6), 067007 (2011).
21. K. K. Bizheva, A. M. Siegel, and D. A. Boas, "Path-length-resolved dynamic light scattering in highly scattering random media: The transition to diffusing wave spectroscopy," Phys. Rev. E Stat. Phys. Plasmas Fluids Relat. Interdiscip. Topics **58**(6), 7664–7667 (1998).
22. A. Wax, C. H. Yang, R. R. Dasari, and M. S. Feld, "Path-length-resolved dynamic light scattering: Modeling the transition from single to diffusive scattering," Appl. Opt. **40**(24), 4222–4227 (2001).
23. R. Carminati, R. Elaloufi, and J. J. Greffet, "Beyond the diffusing-wave spectroscopy model for the temporal fluctuations of scattered light," Phys. Rev. Lett. **92**(21), 213903 (2004).
24. G. Popescu and A. Dogariu, "Optical path-length spectroscopy of wave propagation in random media," Opt. Lett. **24**(7), 442–444 (1999).
25. B. Varghese, V. Rajan, T. G. van Leeuwen, and W. Steenbergen, "Quantification of optical Doppler broadening and optical path lengths of multiply scattered light by phase modulated low coherence interferometry," Opt. Express **15**(15), 9157–9165 (2007).
26. D. A. Boas, K. K. Bizheva, and A. M. Siegel, "Using dynamic low-coherence interferometry to image Brownian motion within highly scattering media," Opt. Lett. **23**(5), 319–321 (1998).
27. Z. P. Chen, T. E. Milner, S. Srinivas, X. J. Wang, A. Malekafzali, M. J. C. van Gemert, and J. S. Nelson, "Noninvasive imaging of in vivo blood flow velocity using optical Doppler tomography," Opt. Lett. **22**(14), 1119–1121 (1997).
28. B. Choi, N. M. Kang, and J. S. Nelson, "Laser speckle imaging for monitoring blood flow dynamics in the in vivo rodent dorsal skin fold model," Microvasc. Res. **68**(2), 143–146 (2004).
29. T. B. Rice, S. D. Konecky, A. Mazhar, D. J. Cuccia, A. J. Durkin, B. Choi, and B. J. Tromberg, "Quantitative determination of dynamical properties using coherent spatial frequency domain imaging," J. Opt. Soc. Am. A **28**(10), 2108–2114 (2011).
30. T. B. Rice, E. Kwan, C. K. Hayakawa, A. J. Durkin, B. Choi, and B. J. Tromberg, "Quantitative, depth-resolved determination of particle motion using multi-exposure, spatial frequency domain laser speckle imaging," Biomed. Opt. Express **4**(12), 2880–2892 (2013).
31. L. Mei, S. Svanberg, and G. Somesfalean, "Frequency-modulated light scattering in colloidal suspensions," Appl. Phys. Lett. **102**(6), 061104 (2013).
32. C. Holt, T. G. Parker, and D. G. Dalgleish, "Measurement of particle sizes by elastic and quasi-elastic light scattering," Biochim. Biophys. Acta **400**(2), 283–292 (1975).
33. R. Finsy, "Particle sizing by quasi-elastic light-scattering," Adv. Colloid. Interfac. **52**, 79–143 (1994).
34. S. G. Anema and Y. M. Li, "Association of denatured whey proteins with casein micelles in heated reconstituted skim milk and its effect on casein micelle size," J. Dairy Res. **70**(1), 73–83 (2003).
35. R. C. Murdock, L. Braydich-Stolle, A. M. Schrand, J. J. Schlager, and S. M. Hussain, "Characterization of nanomaterial dispersion in solution prior to In vitro exposure using dynamic light scattering technique," Toxicol. Sci. **101**(2), 239–253 (2008).
36. Y. Yeh and H. Z. Cummins, "Localized fluid flow measurements with an He-Ne laser spectrometer," Appl. Phys. Lett. **4**, 176–178 (1964).
37. W. Vanmegen and P. N. Pusey, "Dynamic light-scattering study of the glass-transition in a colloidal suspension," Phys. Rev. A **43**(10), 5429–5441 (1991).
38. J. B. Salmon, L. Bécu, S. Manneville, and A. Colin, "Towards local rheology of emulsions under Couette flow using Dynamic Light Scattering," Eur Phys J E Soft Matter **10**(3), 209–221 (2003).
39. M. Berka and J. A. Rice, "Absolute aggregation rate constants in aggregation of kaolinite measured by simultaneous static and dynamic light scattering," Langmuir **20**(15), 6152–6157 (2004).
40. T. Matsunaga and M. Shibayama, "Gel point determination of gelatin hydrogels by dynamic light scattering and rheological measurements," Phys. Rev. E Stat. Nonlin. Soft Matter Phys. **76**(3), 030401 (2007).
41. M. Alexander and D. G. Dalgleish, "Dynamic light scattering techniques and their applications in food science," Food Biophys. **1**(1), 2–13 (2006).

#211079 - $15.00 USD Received 29 Apr 2014; revised 29 Jun 2014; accepted 30 Jun 2014; published 28 Jul 2014

42. D. J. Pine, D. A. Weitz, P. M. Chaikin, and E. Herbolzheimer, "Diffusing wave spectroscopy," Phys. Rev. Lett. **60**(12), 1134–1137 (1988).
43. D. J. Pine, D. A. Weitz, J. X. Zhu, and E. Herbolzheimer, "Diffusing-wave spectroscopy–Dynamic light scattering in the multiple-scattering limit," J. Phys. (Paris) **51**(18), 2101–2127 (1990).
44. D. D. Nolte, *Optical Interferometry for Biology and Medicine*. (Springer, New York, 2011), p.354.
45. H. P. Marshall and G. Koh, "FMCW radars for snow research," Cold Reg. Sci. Technol. **52**(2), 118–131 (2008).
46. P. E. Pace, "FMCW Radar," in *Detecting and classifying low probability of intercept radar* (Artech House, Boston, 2009), 857.
47. W. Eickhoff and R. Ulrich, "Optical frequency-domain reflectometry in single-mode fiber," Appl. Phys. Lett. **39**(9), 693–695 (1981).
48. K. Yuksel, M. Wuilpart, V. Moeyaert, and P. Megret, "Optical frequency domain reflectometry: a review," ICTON: 2009 11th International Conference on Transparent Optical Networks, Vols 1 and 2, 723–727 (2009).
49. Z. G. Guan, P. Lundin, and S. Svanberg, "Assessment of photon migration in scattering media using heterodyning techniques with a frequency modulated diode laser," Opt. Express **17**(18), 16291–16299 (2009).
50. L. Mei, H. Jayaweera, P. Lundin, S. Svanberg, and G. Somesfalean, "Gas spectroscopy and optical path-length assessment in scattering media using a frequency-modulated continuous-wave diode laser," Opt. Lett. **36**(16), 3036–3038 (2011).
51. L. Mei, P. Lundin, S. Andersson-Engels, S. Svanberg, and G. Somesfalean, "Characterization and validation of the frequency-modulated continuous-wave technique for assessment of photon migration in solid scattering media," Appl. Phys. B **109**(3), 467–475 (2012).
52. J. M. Tualle, E. Tinet, and S. Avrillier, "A new and easy way to perform time-resolved measurements of the light scattered by a turbid medium," Opt. Commun. **189**(4-6), 211–220 (2001).
53. J. M. Tualle, H. L. Nghiêm, M. Cheikh, D. Ettori, E. Tinet, and S. Avrillier, "Time-resolved diffusing wave spectroscopy beyond 300 transport mean free paths," J. Opt. Soc. Am. A **23**(6), 1452–1457 (2006).
54. M. Cheikh, H. L. Nghiêm, D. Ettori, E. Tinet, S. Avrillier, and J. M. Tualle, "Time-resolved diffusing wave spectroscopy applied to dynamic heterogeneity imaging," Opt. Lett. **31**(15), 2311–2313 (2006).
55. K. Zarychta, E. Tinet, L. Azizi, S. Avrillier, D. Ettori, and J. M. Tualle, "Time-resolved diffusing wave spectroscopy with a CCD camera," Opt. Express **18**(16), 16289–16301 (2010).
56. J. Zheng, *Optical Frequency-Modulated Continuous-Wave (FMCW) Interferometry* (Springer, 2005).
57. S. R. Arridge, M. Cope, and D. T. Delpy, "The theoretical basis for the determination of optical pathlengths in tissue: temporal and frequency analysis," Phys. Med. Biol. **37**(7), 1531–1560 (1992).
58. A. Giusto, R. Saija, M. A. Iatì, P. Denti, F. Borghese, and O. I. Sindoni, "Optical properties of high-density dispersions of particles: application to intralipid solutions," Appl. Opt. **42**(21), 4375–4380 (2003).
59. R. Michels, F. Foschum, and A. Kienle, "Optical properties of fat emulsions," Opt. Express **16**(8), 5907–5925 (2008).
60. P. D. Ninni, F. Martelli, and G. Zaccanti, "Intralipid: towards a diffusive reference standard for optical tissue phantoms," Phys. Med. Biol. **56**(2), N21–N28 (2011).
61. P. Di Ninni, Y. Bérubé-Lauzière, L. Mercatelli, E. Sani, and F. Martelli, "Fat emulsions as diffusive reference standards for tissue simulating phantoms?" Appl. Opt. **51**(30), 7176–7182 (2012).
62. A. A. Subash, Master's thesis, Lund University, 2012.
63. G. M. Hale and M. R. Querry, "Optical-constants of water in 200-nm to 200-μm wavelength region," Appl. Opt. **12**(3), 555–563 (1973).
64. B. Varghese, V. Rajan, T. G. Van Leeuwen, and W. Steenbergen, "Path-length-resolved measurements of multiple scattered photons in static and dynamic turbid media using phase-modulated low-coherence interferometry," J. Biomed. Opt. **12**(2), 024020 (2007).
65. I. M. Vellekoop and A. P. Mosk, "Phase control algorithms for focusing light through turbid media," Opt. Commun. **281**(11), 3071–3080 (2008).

1. Introduction

As light is irradiated on a turbid medium, it is scattered and absorbed. The scattering and absorption effects can be quantitatively described by the optical properties of the turbid medium, particularly the reduced scattering coefficient and the absorption coefficient. By studying the optical properties of turbid media, one can retrieve the concentrations of the absorbing constituents for, e.g., pharmaceutical tablets [1,2] and wood materials [3]. The optical properties are also highly relevant for, e.g., skin disease assessment [4–6] and tumor/cancer characterization [7–9]. Furthermore, they can be used for modelling light propagation in turbid media, which is particularly useful in biomedical applications [10,11]. Traditionally, there are several experimental approaches which can provide information on the optical properties for turbid media, i.e., time-of-flight spectroscopy (TOFS) [12], the frequency domain photon migration (FDPM) technique [13], and the spatially-resolved diffuse reflectance method [14], etc. The TOFS technique detects the time dispersion (time-

#211079 - $15.00 USD Received 29 Apr 2014; revised 29 Jun 2014; accepted 30 Jun 2014; published 28 Jul 2014

of-flight distribution) of a picosecond light pulse through the sample, while the FDPM technique measures the phase shift of sinusoidally intensity-modulated light traveling through the scattering medium. Of these techniques, the FDPM technique has several attributes that make it well-suited for *in situ* optical properties studies or human diseases assessment. However, the accuracy is generally lower than that of the TOFS technique. Besides, real time phase calibration on the system response is needed for the FDPM technique due to the phase shifts introduced by the instrument such as amplitude-phase cross-talk, which causes inconvenience for real time measurements [15].

Optical properties can also be measured by the low coherent interferometry (LCI) technique [16–20], which examines intensity fluctuations by employing a low-coherence light source. The scattered light – from the ballistic region to the diffusive region – can be clearly resolved by mechanically changing the pathlength of the reference arm [21–23]. By integrating the Doppler power spectrum for each pathlength, the pathlength-resolved photon density function, equivalent to the time-of-flight distribution, can be obtained to retrieve optical properties in dynamic turbid media. However, the signal-to-noise ratio (SNR) is much lower compared with that of the TOFS technique [24,25]. Thus, it is seldom used for optical properties studies. Nevertheless, the LCI technique has been widely used to study the dynamics of turbid media, e.g., Brownian motion [26] and blood perfusion [27], which is difficult for the other methods mentioned above. Actually, apart from utilizing low-coherence light sources, Brownian motion or blood perfusion can also be examined by the so-called laser speckle imaging (LSI) technique with coherent light sources, where the Doppler shifts resulting from the motions of scattering particles are measured [28]. However, the results obtained by the LSI technique are often elusive because of the high scattering in turbid media. Fortunately, such an issue could be solved by introducing the spatial frequency domain imaging technique, where the characteristic path lengths of photons can be controlled [29,30].

Inspired by the rich applied fields of the light scattering techniques outlined above, frequency modulated light scattering interferometry (FMLSI) was recently introduced to study the optical properties and Brownian motion of liquid phantoms by employing a coherent light source [31]. By using a compact and robust free space optical system, FMLSI has achieved promising results. However, the free space FMLSI system limits measurement geometries and thus applications. To overcome such limitations, the present work develops a fiber-based FMLSI system which can be very useful in terms of flexibility especially when measuring biological tissues. The optical properties of both static and dynamic turbid media are studied, and the Brownian diffusion constant of the dynamic turbid samples made from Intralipid® are investigated. The measurement results are compared with predicted values based on published data. The study also includes a discussion of the data analysis procedures and the effect of window functions when performing Fourier transform on the detected light signal, which was not included in the previous work.

2. Theoretical background

In this work, the FMLSI technique deals with scattering media involving both diffusively scattered light and Doppler effects, resulting from Brownian motion. We thus first introduce the basic concept of Brownian motion and relevant techniques; then the FMLSI technique is described in Section 2.2.

2.1. Brownian motion

Brownian motion, widely existing in many turbid media, has attracted considerable interest and found enormous applications. The movement of scattering particles can be detected by the dynamic light scattering (DLS) technique, which examines the intensity fluctuation of singly scattered light (see Fig. 1(a)). The power spectrum of the heterodyne-detected intensity fluctuation is given by a Lorentzian function:

#211079 - $15.00 USD Received 29 Apr 2014; revised 29 Jun 2014; accepted 30 Jun 2014; published 28 Jul 2014

$$S = f_0 \Big/ \left(\pi f^2 + \pi f_0^2\right). \tag{1}$$

here, f_0 is the linewidth of the Lorentzian curve, given by $f_0 = q^2 D_B$ in the single scattering region. q denotes the photon momentum transfer depending on the deflection angle. D_B is the Brownian diffusion constant, depending on the hydrodynamic diameter (a) of the moving particles and viscosity of the turbid medium (η), and can be given by Stokes-Einstein relationship $D_B = k_B T / 3\pi\eta a$. Here k_B is the Boltzmann constant and T is the temperature.

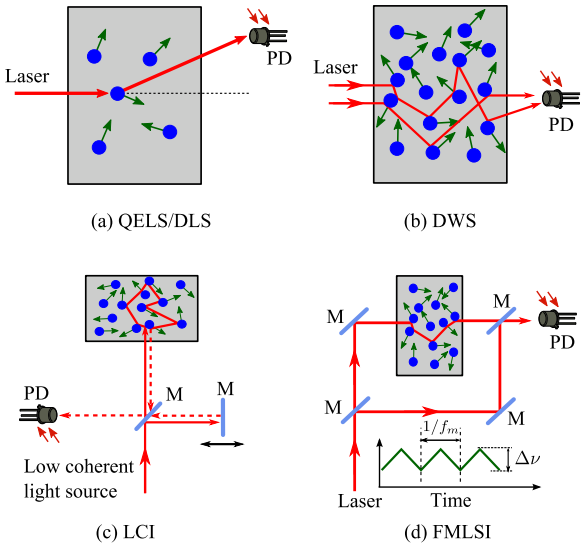

Fig. 1. Schematics of (a) DLS, (b) DWS, (c) LCI and (d) FMLSI techniques. M and PD correspond to mirror (or beam splitter) and photo diode, respectively.

From the Doppler power spectrum of the intensity fluctuation or sometimes from the autocorrelation function, one can retrieve the structure and dynamics of the turbid medium, e.g., particle size [32–35], flow velocity [36], and coagulation and rheology process parameters [37–40]. The major deficiency of DLS is that the condensed sample must be diluted to remain in the single scattering region [41]. Diffusing wave spectroscopy (DWS) [42,43] is thus formulated to deal with multiple or diffusive scattered light (see Fig. 1(b)). The power spectrum for each possible pathlength is integrated in DWS [44], and thus cannot be resolved individually. In practice, the power spectrum measured by the DWS technique depends on the transport mean free path or optical properties [43] which must be determined independently. On the contrary, the LCI technique can measure the power spectrum for each possible path length individually (see Fig. 1(c)).

According to diffusion theory, the pathlength-resolved Doppler power spectrum can also be given by Eq. (1). However, the linewidth f_0 is dependent on the transport mean free path (l^*) and the photon path length ($s = c't$), i.e., $f_0 = k^2 D_B s / \left(\pi l^*\right)$. Here, l^* is the reciprocal of the reduced scattering coefficient (μ_s') of the turbid medium, and c' is the speed of light in the turbid medium.

2.2. Principles of the FMLSI technique

The FMLSI technique, originating from frequency modulated continuous wave (FMCW) radars [45,46] and optical frequency domain reflectometry (OFDR) [47,48], has recently been demonstrated to assess photon migration in turbid media by using tunable diode lasers with a

#211079 - $15.00 USD Received 29 Apr 2014; revised 29 Jun 2014; accepted 30 Jun 2014; published 28 Jul 2014

linearly [31,49–51] or sinusoidally [52–55] chirped optical frequency. However, the movements of the scattering particles must be assumed to be negligible for sinusoidal frequency modulation [54,55], which is not needed for linear frequency scanning. In the present work, we only give a very brief introduction of the FMLSI technique with linear frequency scanning in the case of dynamic turbid media involving Brownian motion.

As shown in Fig. 1(d), by scanning the wavelength/frequency of the light source, beat signals are produced due to time delays between the scattered and reference light waves in the Mach-Zehnder interferometer [56]. Besides, a Doppler shift is generated due to the movement of the scattering particles. Thus, the power spectrum of the detected light intensity is the combined effect of the Doppler shifts and light scattering, from which the optical properties and Brownian diffusion constant can be directly retrieved based on diffusion approximation theory. The power spectrum of the light intensity examined by the FMLSI technique is given by [31]

$$P(f) = \int S[t, f-(t+t_0)\beta]\, \rho(t) dt. \tag{2}$$

Here, $\beta = \Delta\nu f_m$ is the optical frequency modulation coefficient, $\Delta\nu$ is the modulation range, f_m is the modulation frequency, t_0 takes account of the time difference for light traveling in the two arms of the interferometer. $S(t, f)$ corresponds to the pathlength-resolved Doppler power spectrum measured by LCI with a path length of $s = c't$. From Eq. (2), it can be seen that the power spectrum examined by the FMLSI technique is actually the accumulation of the Doppler spectra for all possible pathlengths. However, the accumulation is frequency shifted due to the linear frequency modulation in the FMLSI technique. Thus, the information of light scattering is retained, which is not the case for the DWS techniques.

In the case of an infinite medium, the detected light intensity with a source-detector separation of r can be simply described by the diffusion approximation theory:

$$\rho(r,t) = \frac{c'}{4\pi}\left(\frac{1}{4\pi Dc't}\right)^{3/2} \exp(-\mu_a c't - \frac{r^2}{4Dc't}). \tag{3}$$

Here, D is the optical diffusion coefficient given by $D = 1/\left[3(\mu_s' + \mu_a)\right]$. For the time-of-flight distribution in other geometries, the reader is referred to [57]. However, it is important to note that the diffusion approximation theory is mainly valid for the cases when scattering is dominant over absorption and the source-detector separation is sufficiently large ($r > 10l^*$). By modeling Eq. (2), the reduced scattering coefficient and absorption coefficient can be separated and the Brownian diffusion constant of the turbid medium is also retrieved. For a static turbid medium, the power spectrum of the Brownian motion can be replaced by a Dirac delta function, as discussed in [31].

3. Materials and methods

3.1. Instrumentation

The system schematic is given in Fig. 2. A tunable DFB diode laser (EYP-DFB-0852-00150-1500-TOC03) running at 852 nm is utilized as a light source. The typical linewidth of the diode laser is 2 MHz, providing a coherence length up to 150 m in free space. The wavelength/frequency of the laser diode is scanned in a repetition frequency of 400 Hz with triangular waveform. The corresponding optical tuning range is $\Delta\nu = 60$ GHz. The output laser beam is first collimated and then divided into two paths: one path is coupled into a graded index multimode fiber (600 μm core diameter) to illuminate the sample, and the other part is guided directly into the interferometer. Scattered light is collected by another graded index multimode fiber with 100 μm core diameter, and collimated before coupled together

#211079 - $15.00 USD Received 29 Apr 2014; revised 29 Jun 2014; accepted 30 Jun 2014; published 28 Jul 2014

with the reference arm. The beat signal is detected by an avalanche photodiode (APD, API, APD-SD384-70-72-661), amplified by a low-noise amplifier (SRS Model SR560) with a band-pass filter (10 kHz – 10 MHz). The light signal is then sampled by a data acquisition card (NI 6132) with a sampling frequency of 2.5 MHz, and the digitized data are transferred to a computer for analysis. The reason for using a triangular wave instead of a saw-tooth wave is that the intensity of the harmonics of the triangular wave decreases much faster, giving much smaller effect on the power spectrum, and sets lower requirement on the electronics. We should note that the equivalent modulation frequency f_m is then 800 Hz when using 400-Hz triangular modulation.

Using multimode fibers to deliver and collect light is particularly convenient for optical properties and dynamics studies for many applications, as shown in Fig. 2. Static samples can then be measured in reflectance or transmittance geometries. The dynamic turbid samples can be measured by inserting the multimode fibers deep down into the medium, to perform measurements with infinite geometry. However, one must carefully align the system to avoid optical interference fringes originating from the surfaces of the optics. In practice, when coupling light into the delivery fiber with 600 μm core diameter, it is much easier to eliminate spurious interference fringes compared to the case of a 100 μm fiber, when considering a high coupling efficiency. However, the 600 μm multimode fiber may induce the risk of increased time dispersion, although the time dispersion of a graded index multimode fiber should in principle not depend on the core diameter of fibers. The main reason of using a 100 μm collection fiber is to match the beam sizes of the reference arm and the fiber with less optics, which can minimize the interference fringes resulting from the surfaces of optics. However, one can definitely use collection fiber with even larger core diameter if the interference fringes originating from the surfaces of optical components can be efficiently suppressed. In the current system, an optical isolator is used both for protecting the diode laser and reducing the interference fringes.

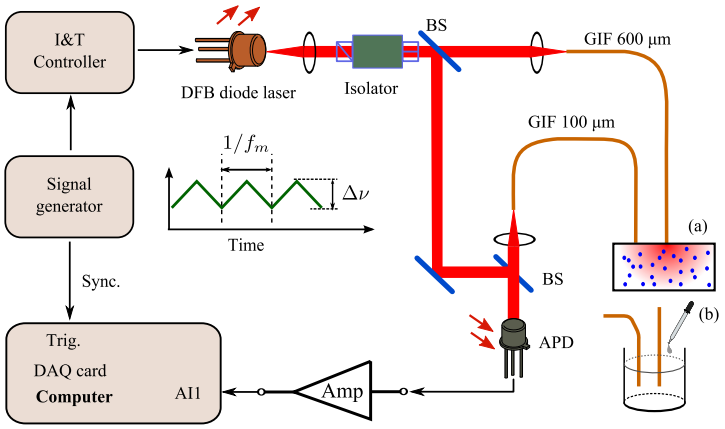

Fig. 2. Schematic of the fiber based FMLSI system, (a) reflectance measurement for a static medium, and (b) dynamic turbid medium measured in an infinite geometry.

3.2. Data analysis

When digitizing the beat signal, the effective sampling time (T_s) is normally slightly shorter than the modulation period (1.25 ms), i.e., T_s = 1 ms, to avoid a sharp edge due to the modulation pattern. Thus, the frequency bin of the Fourier transform is $1/T_s$ = 1 kHz, which gives a time resolution of $1/\beta T_s = 21$ ps for the present FMLSI system. If we denote the detected light intensity as $I(T_s, t)$, the corresponding power spectrum can be calculated as

#211079 - $15.00 USD Received 29 Apr 2014; revised 29 Jun 2014; accepted 30 Jun 2014; published 28 Jul 2014

$$P_I(f) = \left\langle \left| \mathcal{F}\left[I(T_s,t) w(T_s,t) \right] \right|^2 \right\rangle. \quad (4)$$

here, $\langle\ \rangle$ denotes the ensemble average of the power spectrum, and $w(T_s,t)$ is the window function to reduce frequency leakage due to non-integral data sampling, which is an intrinsic problem of the digital Fourier transform (DFT). Typical window functions are, e.g., rectangular, Hanning or Hamming windows. In our previous work, a rectangular window function was used [31]. In this work, we study the effect of applying different window functions. The main characteristics of window functions are the suppression of the maximum side lobes and the effective bandwidth B (or frequency bin). Here we investigate the effect of three different window functions: rectangular (B = 1), exponential (B = 1.08), and Hamming window functions (B = 1.37). Generally, larger suppression of side lobes corresponds to a larger bandwidth (B), giving a reduced frequency resolution.

The background power spectrum, which can be recorded by blocking the collection fiber, must be subtracted from the power spectrum measured through the samples. The frequency offset $t_0\beta$ can be measured by sending light through a paper, which has a negligible path length, before being collected by the multimode fiber. The value of $t_0\beta$ is 65 kHz in the current system. The obtained power spectrum is then referred to as the instrument response function (IRF, $R(f)$). IRF normally has a certain spectral width, resulting from, e.g., mode dispersion in the graded index fiber, non-infinitely narrow laser linewidth, and frequency leakage. The nonlinear fitting process can then be performed according to the following equation

$$P_I(f) = A_1 \int P(f')R(f'-f)df'. \quad (5)$$

here, A_1 is a scaling factor. Based on Eqs. (4) and (5), the optical properties and the Brownian diffusion constant can be obtained.

3.3. Materials

3.3.1. Polystyrene foam

The static turbid medium examined here is a 12-mm polystyrene foam with extremely high porosity (98%). The value of μ_s' is typically between 33 to 36 cm^{-1}, while the absorption coefficient is negligible compared to the reduced scattering coefficient [51]. The effective refractive index of polystyrene foam is about 1.01 [15].

3.3.2. Intralipid phantoms

In the present work, 20% Intralipid (0.2 g per mL, Batch 10GC9599), made up of 20% soybean oil, 1.2% egg yolk phospholipids, 2.25% glycerin, and water (Fresenius Kabi AB, Uppsala, Sweden), was used as scattering particles and was diluted to prepare dynamic phantom samples. Six samples were prepared by first mixing 35 ml 20% Intralipid with 550-ml water and then continuously adding 5-ml Intralipid into the glass container until 60 ml 20% Intralipid was reached in total. The corresponding Intralipid mass concentrations were 1.21%, 1.37%, 1.54%, 1.69%, 1.85% and 2.01% (g/ml).

In order to verify the experimental results, we hereby try to estimate the values of optical properties and the Brownian diffusion constant based on relevant data published by other researchers. Intralipid, which has been carefully studied by many groups [58–62], is very popular as standard tissue phantoms for various biomedical applications. In this work, the optical properties for the 20% Intralipid studied recently by Di Ninni *et al.* [60,61], are used as references. The value of μ_s' is wavelength dependent, and is estimated to be 180 cm^{-1} at 852 nm, which are quite close (a few percent difference) to the results measured by the TOFS

#211079 - $15.00 USD Received 29 Apr 2014; revised 29 Jun 2014; accepted 30 Jun 2014; published 28 Jul 2014

technique [62]. The values of μ_s' for the diluted Intralipid phantom samples with a mass concentration of ϕ (g/ml) can be simply estimated as

$$\mu_s'(\phi) = \mu_s'(0.2\text{g/ml})\frac{\phi}{0.2\text{g/ml}} \tag{6}$$

According to the above equation, the values of μ_s' will vary from 10.8 to 18.0 cm^{-1}. The absorption coefficient of Intralipid is quite low in this wavelength region [61]. Thus, the absorption of the diluted Intralipid phantoms is mainly due to water, with an absorption coefficient of around 0.043 cm^{-1} [63]. Thus, the requirement for the validity of the diffusion approximation theory is satisfied for the dynamic samples when the source-detector separation is in the order of 10 mm.

To estimate the value of Brownian diffusion constant D_B, viscosity and hydrodynamic diameter are the two key parameters. The viscosity (η) of the turbid medium linearly increases with the particle volume fraction (ϕ_V) for extremely low particle volume concentrations, i.e., $\eta = (1+2.5\phi_V)\eta_{water}(T)$; here $\eta_{water}(T)$ is the viscosity of water at the temperature T. The value of ϕ_V is very close to the mass concentration since the density of Intralipid is close to 1 [59]. Obviously, the value of the viscosity only increases a few percent for the extremely low Intralipid concentrations and the viscosity of water can be used as an approximation of the viscosity for all Intralipid samples. Based on the above discussions, an estimated viscosity of the Intralipid phantom samples can be obtained, i.e., 1.0×10^{-3} Pa·s at room temperature (20°C). For the hydrodynamic diameter/radius of the scattering particles, the physical particle size, varying from 25 nm up to hundreds of nm for the 20% Intralipid, can be used as an approximation for the hydrodynamic diameter, i.e., 0.12 μm which is calculated from the weighted average of Eq. (7) in [59]. Thus, the Brownian diffusion constant can be calculated, i.e., 3.6×10^{-12} m^2/s.

4. Results and discussion

4.1. Static turbid media measurements

Figure 3 shows the power spectra of a polystyrene foam measured in transmission geometry. Without any vibration, the power spectrum shows many spikes and is difficult to model. This is also what we expect based on previous work [51]. However, after manually vibrating the collection fiber, which generates a random interference speckle pattern, the power spectrum is smoothed. The nonlinear fitting, performed in the region between 74 kHz to 134 kHz, gives a reduced scattering coefficient of 34 cm^{-1}, and a negligible absorption coefficient, which is in good agreement with the results obtained by the TOFS system [51].

#211079 - $15.00 USD Received 29 Apr 2014; revised 29 Jun 2014; accepted 30 Jun 2014; published 28 Jul 2014

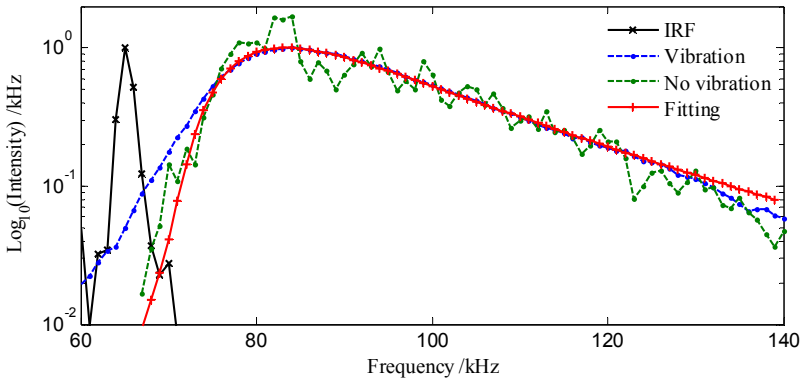

Fig. 3. Power spectra (plotted in logarithmic scale) of a 12-mm polystyrene foam measured in transmission geometry.

As can be seen from Fig. 3, the fits are worse for the high-frequency region when the intensity of the power spectrum is decreased. Notably, the measured and fitted power spectra show large discrepancies in the low-frequency region. The deviation can be attributed to the vibration of the collection fiber, which may induce extra time dispersion and frequency leakage. Actually, we can even observe that the power spectrum is broadened in the low-frequency region after vibration. To reduce the discrepancies and obtain a smooth power spectrum, alternatively, one can randomly vibrate the illumination fiber on a very small scale to smooth the power spectrum as demonstrated in [52]. Another way to obtain a smooth power spectrum is to randomly change the phase of the reference light wave. This method has been utilized to study static turbid media with LCI techniques [64]. In practice, similar techniques have been used to change the phase term or wave front to focus a light beam after propagation in turbid media [65]. Despite that the results render discrepancies in low-frequency fitting, however, the agreement between the measured values and previous work show great potential for using the FMLSI technique for optical properties studies on static turbid media.

4.2. Dynamic turbid media measurements

The power spectra for several Intralipid samples and the corresponding fitting results are shown in Fig. 4. The samples are measured in an infinite geometry with source-detector separation of 12 mm. Not surprisingly, the power spectra are quite smooth due to the movement of the scattering particles. The peaks of the power spectra shift to higher frequency with increased reduced scattering coefficients. The fitting range starts from 65 kHz and ends up at the frequencies where the corresponding intensities are around 20% of the peak intensity. As can be seen from Fig. 4, very promising fitting results are obtained by employing a Hamming window function. The fitting values of the optical properties and the Brownian diffusion constants are given in Fig. 5. The slightly larger values of μ_s' compared with the estimated values are due to, e.g., source-detector separation errors and measurement errors of the modulation frequency. Notably, similar error sources also exist in the TOFS technique. Nevertheless, the values of μ_s' follow the variations of the estimated values.

#211079 - $15.00 USD Received 29 Apr 2014; revised 29 Jun 2014; accepted 30 Jun 2014; published 28 Jul 2014

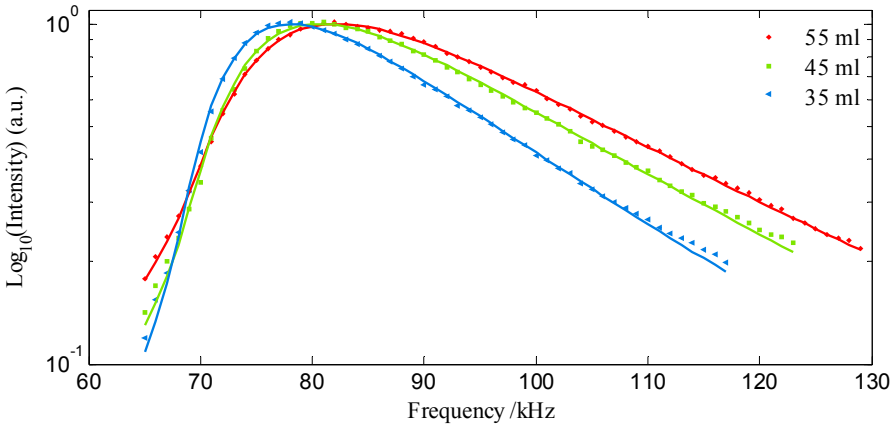

Fig. 4. Power spectra (plotted in logarithmic scale) for samples with different Intralipid concentrations (volumes).

The measured values of μ_a are larger than that for water, but the variations are small. Although the experimental noise is, generally speaking, at a low level, it can still result in fitting errors or variations on the values of μ_a and μ_s', due to the relatively strong coupling between μ_s' and μ_a. After fixing the values of μ_a to the average value, i.e., 0.068 cm^{-1}, the fitting values of μ_s' show even better linearity, as can be seen from Fig. 5(a); however, the values of the Brownian diffusion constant D_B do not change. It can be mentioned that we also further fixed the value of D_B to the average value, i.e., 1.9 × 10^{-12} m^2/s; however, the linearity of the values of μ_s' did not improve any more. This indicates that the coupling between the Brownian diffusion constant and reduced scattering coefficient is very weak. Moreover, we should note that a larger Brownian diffusion constant will give a broader power spectrum while a larger absorption coefficient can kill photons with longer path lengths and thus narrow the power spectrum. In practice, it seems that the absorption coefficient and the Brownian diffusion constant are entangled, as shown in Fig. 5(b). The variations (± 11%) of the Brownian diffusion constant can be attributed to fitting errors, experimental noise, and variations of the dynamics of the samples.

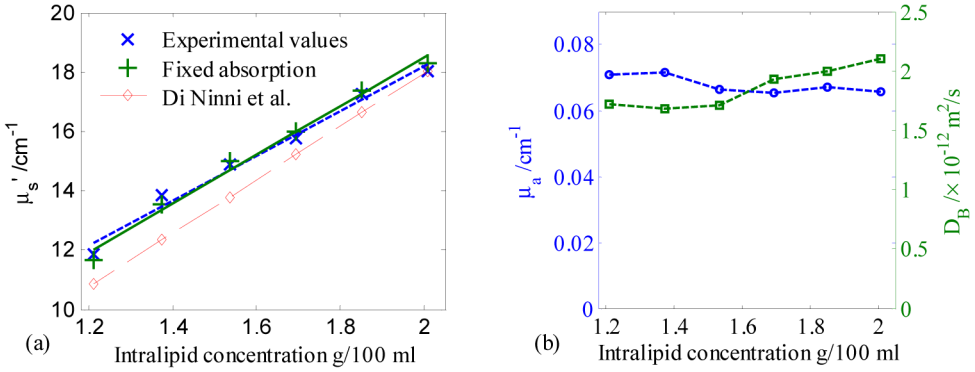

Fig. 5. (a) Reduced scattering coefficients, (b) absorption coefficients and Brownian diffusion constants for liquid phantoms with different Intralipid concentrations when employing a Hamming window function. The corresponding estimated values given in Section 3.3.2 are 0.043 cm^{-1} (μ_a) and 3.6 × 10^{-12} m^2/s (D_B), respectively.

#211079 - $15.00 USD Received 29 Apr 2014; revised 29 Jun 2014; accepted 30 Jun 2014; published 28 Jul 2014

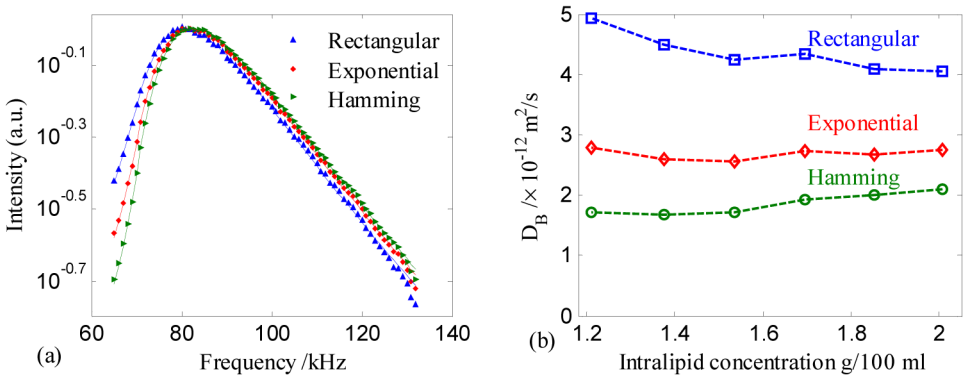

Fig. 6. (a) Power spectra for 60-ml 20% Intralipid sample (plotted in logarithmic scale) with different window functions. The rectangular window function works better for the low-frequency region, while the Hamming window function has better performance for the high-frequency region; (b) Brownian diffusion constants obtained for different window functions, the corresponding mean values and standard variations are $4.4 \pm 0.3 \times 10^{-12}$ m^2/s (rectangular), $2.7 \pm 0.1 \times 10^{-12}$ m^2/s (exponential) $1.9 \pm 0.2 \times 10^{-12}$ m^2/s (Hamming).

When applying different window functions on the detected light signal, the resulted power spectra are significantly different, as can be seen from Fig. 6(a). However, the variations of the values of μ_s' are generally less than 2%. The values of μ_a are 0.099 ± 0.003 cm^{-1} (rectangular), 0.079 ± 002 cm^{-1} (exponential), and 0.068 ± 0.003 cm^{-1} (Hamming). As is well-known, the absorption coefficient mainly affects the slope of the time-of-flight distribution. Coincidentally, we clearly see that the slope of the power spectrum changes when employing different window functions, which is the main reason why the variation of μ_a is much larger compared to that of μ_s'. We also note that the percentage errors of the fits are different when applying different window functions, which could also contribute the variations of the fitting results.

Significant differences occur for the values of the Brownian diffusion constant when applying different window functions, as shown in Fig. 6(b). As can be seen, the values of D_B decrease as the power spectra become narrower and shift to the higher-frequency region when employing different window functions. Such variations are reasonable, since the effect of Brownian motion is to introduce a broadening on the time-of-flight distribution, as described by Eq. (2). Such an effect is quite similar to the one resulting from the window function given in Eq. (4), which is equivalent to a convolution in the frequency domain.

The large variation substantially increases the difficulties in studying the Brownian motion from the power spectrum. From Fig. 6(b), it can be seen that Brownian diffusion constants obtained with the exponential window function have the lowest variation, and are close to what has been estimated in Section 3.2. Notably, the absorption coefficients also have the lowest variation. Based on these observations, we can conclude that the exponential window function should probably be used for data analysis to obtain reasonable values of the Brownian diffusion constant. However, careful calibration of the Brownian diffusion constant with other techniques should be performed to confirm this conclusion.

Based on the above discussion, the uncertainties of the fitting values when employing the exponential window function are also investigated. As shown in Table 1, we can observe a clear increasing trend of fitting uncertainties when the scattering coefficient or Intralipid volume is decreased. This indicates that the increase of fitting uncertainties is related to the validity of the diffusion approximation theory. Besides, another major uncertainty of the extracted values originates from the measurement error of source-detector separation. It is found out that if the source-detector separation varies ± 0.5 mm around 12 mm, the maximum

#211079 - $15.00 USD Received 29 Apr 2014; revised 29 Jun 2014; accepted 30 Jun 2014; published 28 Jul 2014

variations of the extracted parameters are ± 8.9% (μ_s'),± 0.0% (μ_a), and ± 8.5% (D_B). Considering also the error resulting from source-detector separation, the overall errors/uncertainties can be estimated, i.e., ± 10% (μ_s'), ± 12% (μ_a), and ± 12% (D_B). However, to be noted, the uncertainties discussed here can be further reduced by, e.g., employing Monte Carlo simulation or reduce the percentage error of the source-detector separation.

Table 1. Fitting errors of optical properties and Brownian diffusion constant when employing an exponential window function.

Intralipid volume/ ml	60	55	50	45	40	35
μ_s' fitting uncertainties (±/%)	2.3	2.1	2.5	3.2	3.2	3.6
μ_a fitting uncertainties (±/%)	6.5	6.1	7.4	9.7	9.7	11.7
D_B fitting uncertainties (±/%)	3.7	3.8	4.6	7.3	7.7	9.0

5. Conclusions

We prove that a fiber-based FMLSI system can be very useful for optical properties studies, both for static and dynamic turbid media involving Brownian motion. The optical properties obtained in this study show good agreement with published work. We suggest that, for other dynamic turbid media where the scattering particles exhibit, e.g., directional movement, the theoretical model mentioned above should be modified to take this into account. By using the statistical method – Monte Carlo simulation, one can, in principle, model any type of dynamic turbid media. On the other hand, one can increase the modulation frequency, which could then freeze the movement of the scattering particles, and the optical properties can be readily obtained without considering the Doppler effect.

Brownian diffusion constants are also investigated in this work. It is found that the measured values are significantly affected by the frequency leakage. Different window functions result in completely different values of D_B; however, the optical properties do not change too much, especially for the reduced scattering coefficient. Based on the present work, we conclude that the exponential window function can give promising results. However, this must be further confirmed, e.g., by performing careful DWS studies on the liquid phantoms. If the presented results can be verified, the FMLSI technique is a promising technique for general colloidal suspension studies, since it can directly obtain the Brownian diffusion constant while the DWS technique requires independent measurement of the reduced scattering coefficient.

Acknowledgments

The authors gratefully acknowledge Stefan Andersson-Engels for discussions, Katarina Svanberg for providing Intralipid, and Lene Nordrum for language review. This work was supported by a direct Swedish Research Council grant (621-2011-4265), a Linnaeus grant to the Lund Laser Centre, and by the Safetypack project.

#211079 - $15.00 USD Received 29 Apr 2014; revised 29 Jun 2014; accepted 30 Jun 2014; published 28 Jul 2014